

Article

Mineralogy and Geochemical Characteristics of Scheelite Deposit at Xuebaoding in Pingwu, Sichuan Province, China

Qinyuan Cao ¹, Miao Shi ^{1,2,3,*}, Ye Yuan ⁴, Shiyu Ma ¹ and Haoyu Lu ¹

- ¹ School of Earth Sciences, Hebei GEO University, Shijiazhuang 050031, China; maxcaoqinyuan@163.com (Q.C.); masy0107@163.com (S.M.); 118866545749@163.com (H.L.)
- ² Hebei Key Laboratory of Green Development of Rock Mineral Materials, Hebei GEO University, Shijiazhuang 050031, China
- ³ Engineering Research Center for Silicate Solid Waste Resource Utilization of Hebei Province, Hebei GEO University, Shijiazhuang 050031, China
- ⁴ School of Gemmology, China University of Geosciences, Beijing 100083, China; yuenyeah@163.com
- * Correspondence: miaoer727@126.com; Tel.: +86-0311-8720-8485

Abstract: Featuring subtle lithological alterations in the host rocks and containing colossal gemstone crystals, the scheelite deposit at Xuebaoding in the Pingwu region of Sichuan Province exhibits characteristics typical of a vein-like hydrothermal-type deposit. The scheelite from the Xuebaoding region is renowned for its high saturation of color, perfect crystal shape, and pure color. In this study, its crystal structure and mineralogical, geochemical, and in situ Sr-Nd isotope characteristics are all systematically characterized. Our objective is to determine the source of ore-forming materials, the timing of the mineralization, and the chemical composition of scheelite, including major elements, trace elements, and rare earths elements (REE). The scheelite samples were analyzed with a variety of methods such as polarizing microscopy, X-ray powder diffraction (XRD), X-ray fluorescence spectrometry (XRF), electron probing, and laser ablation inductively coupled plasma mass spectrometry (LA-ICP-MS). In addition, conventional gemological tests were performed using instruments including gemstone microscopes, GI-UVB ultraviolet fluorescent lamps, grating spectroscopy, etc. The results demonstrate that scheelite exhibits a high refractive index, excellent crystallinity, and a granular structure. Clear color bands and ring structures are observed within the minerals, accompanied by interference colors of light blue, blue, and yellow. Additionally, the mineral components are relatively concentrated, with muscovite and illite serving as accessory minerals. Furthermore, the chemical composition of scheelite reveals a WO_3/CaO mass ratio that approaches or exceeds the ideal value. Moreover, it exhibits a wide range of variations in total rare earth element (ΣREE) content, which is characterized by an enrichment of light rare earths (LREE), significant negative Eu anomalies, and insignificant Ce anomalies. In addition, the metallogenic formation of scheelite can be estimated to have occurred during the Toarcian stage in the Lower Jurassic Epoch period, approximately 183 Ma. The study further revealed that A-type granite serves as the genesis type of scheelite, with most of the ore-forming materials originating from the upper crust and a few derived from younger crustal sources.

Keywords: Xuebaoding; scheelite; mineralogy characteristics; in situ elements analysis; Sr-Nd isotopes



Citation: Cao, Q.; Shi, M.; Yuan, Y.; Ma, S.; Lu, H. Mineralogy and Geochemical Characteristics of Scheelite Deposit at Xuebaoding in Pingwu, Sichuan Province, China. *Minerals* **2024**, *14*, 38. <https://doi.org/10.3390/min14010038>

Academic Editor: Anthony Bell

Received: 16 November 2023

Revised: 17 December 2023

Accepted: 19 December 2023

Published: 28 December 2023



Copyright: © 2023 by the authors. Licensee MDPI, Basel, Switzerland. This article is an open access article distributed under the terms and conditions of the Creative Commons Attribution (CC BY) license (<https://creativecommons.org/licenses/by/4.0/>).

1. Introduction

Scheelite is a commonly occurring tungstate mineral and an anhydrous compound with the chemical formula $Ca[WO_4]$, belonging to the tetragonal crystal system. Key characteristics of scheelite include an island structure, a greasy luster, and transparency to translucency. Scheelite occurs in skarn, pegmatites, and hydrothermal veins with high to moderate temperatures [1]. Notably, scheelite is also an important mineral for understanding varieties of geologically diverse ore deposit setting, including porphyries,

vein/stockworks, greisens and orogenic Au deposits [2–5]. As a significant tungsten producer, China possesses over 60% of the world's tungsten resources. Among these resources, the reserves and mining output of scheelite consistently ranked first globally [6].

The tungsten–tin–beryllium (W–Sn–Be) deposit in Xuebaoding is located on the northern margin of the Western Longmen Mountains, representing the sole deposit discovered to date. Within the Songpan Ganzi and Qinling orogenic belts, it constitutes a hydrothermal vein deposit formed at high to medium temperatures with W, Sn and Be as its primary elements found in the ore. The deposit is predominantly located within tensile fractures in marble positioned between Pankou and Pukouling granites. The ore veins are composed of beryl, cassiterite, and muscovite within the granite. Meanwhile, the veins are surrounded by rocks composed of marble, which contain beryl, scheelite, cassiterite, and quartz. The scheelite produced from this deposit exhibits relatively large crystals, a beautiful appearance, and reaches gemstone grade [7,8].

Extensive research has been conducted by previous scholars on the scheelite from Xuebaoding. In terms of gemological and mineralogical characteristics [9], study has focused on orange toned scheelite, which exhibits translucency, a greasy luster, and strong blue and white fluorescence observed at short wavelengths (S.W.), as well as good crystallinity. Vibration spectroscopy has been employed to investigate the color genesis of orange–red, orange–yellow, and colorless scheelite [10]. According to the crystal field theory, the color genesis of scheelite from Xuebaoding may be related to the smaller microstructure within the crystal structure, as well as trace elements and REEs. In addition, most research efforts have primarily concentrated on the W–Sn–Be deposit in Xuebaoding [7,11], encompassing investigations into the individual mineral characteristics, mineral zonation features, metallogenic age determination, analysis of metallogenic properties, and exploration of the formation mechanism of the Xuebaoding deposit. Nevertheless, there has been relatively limited research on the scheelite with different color tones in this region.

The present study reveals the gemological and mineralogical characteristics, rare-earth patterns, genesis types, and the timing of the mineralization of scheelite. These findings provided the scientific basis for the identification and prospecting of scheelite from Xuebaoding, thereby enriching the geochemistry and geochronological research content concerning scheelite.

2. Regional Geological Setting

Xuebaoding peak, located at 103.8° E and 32.7° N in Songpan County, Aba Tibetan Autonomous Prefecture, reaches an impressive altitude of 5588 m. As the highest summit in the Minshan mountain range, it stands in the southern section, which extends from north to south. The region below 5000 m elevation is primarily composed of rocky terrain, with the primary peak constituted by carboniferous limestone. The W–Sn–Be gemstone deposit in Pingwu, Sichuan Province, is produced in Moziping, the east–west complex tectonic belt of the Motianling, and is the secondary structure of the upper nano–complex syncline core located in the Zibaishan dome tectonics. The predominantly exposed strata within the mining area encompass the Lower Triassic Bocigou Formation (T_1b), the Middle Triassic Zanaishan Formation (T_2z), and the Upper Triassic Jurassic Formation (T_3zh). Among them, the Zanaishan Formation represents a sequence of metamorphic clastic rock mixed with carbonate rocks, which serve as the main ore-bearing layer of the W–Sn–Be deposit in Xuebaoding [12]. The exposed magmatic rocks in this region predominantly consist of granite with a high content of WO_3^{2-} , and certain veins are directly situated within the granite mass, which indicates a genetic connection between the late Indosinian to early Yanshan magmatic activity and W–Sn–Be mineralization [13]. In addition, the Upper Triassic Jurassic Formation is mainly composed of slate, schist, and marble, which serve as one of the main perimeter rocks of the W–Sn–Be ore body in Xuebaoding [14]. The lower section of the Zagunao Formation in the Middle Triassic can be divided into eight layers from bottom to top, consisting of phyllite and marble from the shallow metamorphic rock series. Furthermore, the magmatic rocks in the region are a group of granite bodies intruded

in the late Indosinian period, which are well developed and occur as rock stocks and veins. Among the rock bodies closely associated with W-Sn-Be mineralization, the most prominent one is Zibaishan rock, which exhibits excellent exposure [8]. The Xuebaoding deposit primarily occurs within a monocline stratum formation at the contact between granite and marble in the Pankou and Pukouling Mountains [7].

3. Materials and Methods

3.1. Materials

In the study, five scheelite samples were tested, including three raw samples with a light yellow to orange tone, a nearly colorless sample with quartz as the accessory mineral, and a light yellow tone sample with muscovite as the accessory mineral (Figure 1). The samples were categorized into two groups: the first group was named raw scheelite (R-Sch), with samples labeled Sch-1, Sch-2, and Sch-3, while the second group was named accessory minerals, with scheelite (A-Sch) samples labeled as Sch-4 and Sch-5.

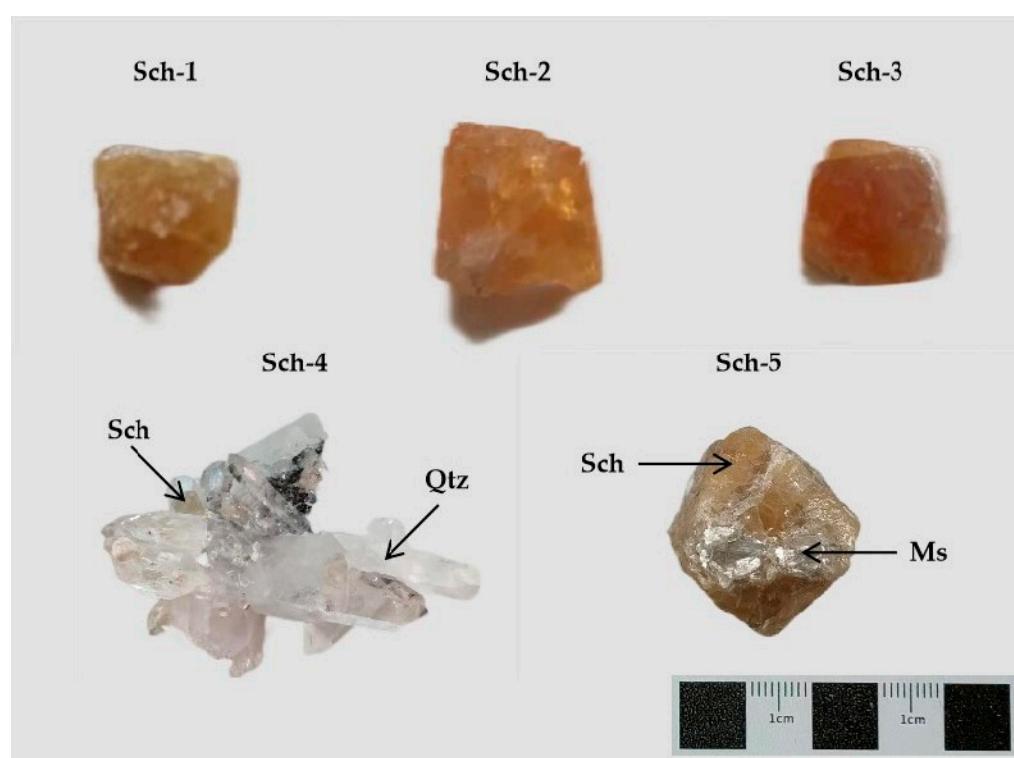


Figure 1. Samples of scheelite from Xuebaoding. R-Sch samples: Sch-1, Sch-2, and Sch-3 (light yellow to orange tone). A-Sch samples as Sch-4 (transparency and nearly colorless), and Sch-5 (translucent and light yellow tone). R-Sch: raw scheelite A-Sch: accessory minerals with scheelite Sch: scheelite Qtz: quartz Ms: muscovite.

3.2. Methods

A conventional gemstone mineralogy testing experiment was conducted at the Hebei Key Laboratory of Green Development of Rock Mineral Materials. Experimental instruments used included gemstone microscope, polarizing microscope, electronic balance, GI-UVB ultraviolet fluorescent lamp, polar scope, and grating spectroscopy. The experiments were carried out under conditions of room temperature at 27.2 °C and an air humidity level of 10%.

X-ray powder diffraction (XRD) experimental testing of the A-Sch samples was completed in the Hebei Key Laboratory of Green Development of Rock Mineral Materials. The experimental instrument used was a Rigaku 9 kW X-ray diffraction analyzer from the Nippon Institute of Science. Experimental conditions with the sample were ground

to 200 mesh and the experiment employed a Cu target, K α radiation, a working voltage of 45 kV, and a working current of 200 mA. Scanning was performed within the range of 3° – 90° (2θ), with a scanning speed set at 10° (2θ /min, continuous scanning).

X-ray fluorescence spectroscopy (XRF) experiment was conducted at the Gemology Experimental Teaching Center of China University of Geosciences (Beijing), where non-destructive testing and analysis were performed on R–Sch samples. The experimental instrument used was the SHIMADZU EDX-7000 energy dispersive X-ray fluorescence spectrometer from Japan. Experimental conditions included Rh target, 5 mm collimator, a testing element range of 11Na–92U, testing voltages of 15 kV (Na-SC) and 50 kV (Al-U), and a testing current of 1000 μ A. The basic parameter method (FP method) was adopted, with the testing environment maintained in a vacuum atmosphere.

An electron probe experiment was conducted at the Hebei Key Laboratory of Green Development of Rock Mineral Materials. Two groups of samples were tested for 15 points and precise data points were obtained for subsequent analysis. The experimental instrument used was the JEOL-JXA-8230 electronic probe manufactured in Japan. Experimental conditions included an acceleration voltage of 15 kV, a working current of 20 nA, and a beam spot diameter of 5 μ m. Regarding integration time, the main elements (content of more than 1 wt.%) were measured for 10 s with background measurements taken for 5 s, the trace elements (content of less than 1 wt.%) took 20 s, and the background takes 10 s.

LA-ICP-MS tests and experimental analysis were completed in the Hebei Key Laboratory of Strategic Critical Mineral Resources. Two groups of samples were analyzed at 30 different points, yielding precise data for further analysis. The experimental setup involved the utilization of the Thermo iCAP RQ ICP-MS inductively coupled plasma mass spectrometer in conjunction with a 193 nm ArF laser sourced from the United States. Experimental parameters included a laser beam diameter of 29 mm and a repetition frequency of 6 Hz. NIST 610 was employed as an external standard, while Ca served as an internal standard element.

An in situ Sr-Nd isotope testing experiment was successfully conducted at the Hebei Key Laboratory of Strategic Critical Mineral Resources. Two groups of samples were analyzed at 15 different points, and precise data points were obtained for further analysis. The experimental instrument employed was an LA-MC-ICP-MS equipped with a 193 nm laser. Experimental conditions included a beam spot size of 43 μ , an energy level of 6 J, and a frequency of 5 Hz.

4. Results

4.1. Gemological Mineralogy Characteristics of Scheelite from Xuebaoding

4.1.1. Gemological Characteristics

Two groups of scheelite samples were subjected to magnified observations, revealing clear color bands could be observed inside the R–Sch samples with light yellow to orange tone, with some samples exhibiting relatively clean interiors (Figure 2a–c). The A–Sch samples displayed growth morphology, dark inclusions, and ring structures, while the accessory mineral muscovite was visible to the naked eye (Figure 2d–f).

The routine test results indicated that scheelite exhibits a greasy luster, varying degrees of transparency, a range from translucency to transparency, with density falling within the normal range for scheelite (5.8–6.2) g/cm^3 [15]. Through an orthogonal polarizing microscope, non-homogeneous characteristics were suggested by four bright and four dark extinction phenomena observed in this gemstone. Grating the spectroscopy analysis revealed absorption lines primarily in the yellow and green regions, with a weak Nd element absorption line detected at 584 nm. The nearly colorless scheelite sample showed no absorption line in the yellow region. However, the yellow tone scheelite sample exhibited absorption lines, regardless of whether the color tone was dark or light (see Table 1).

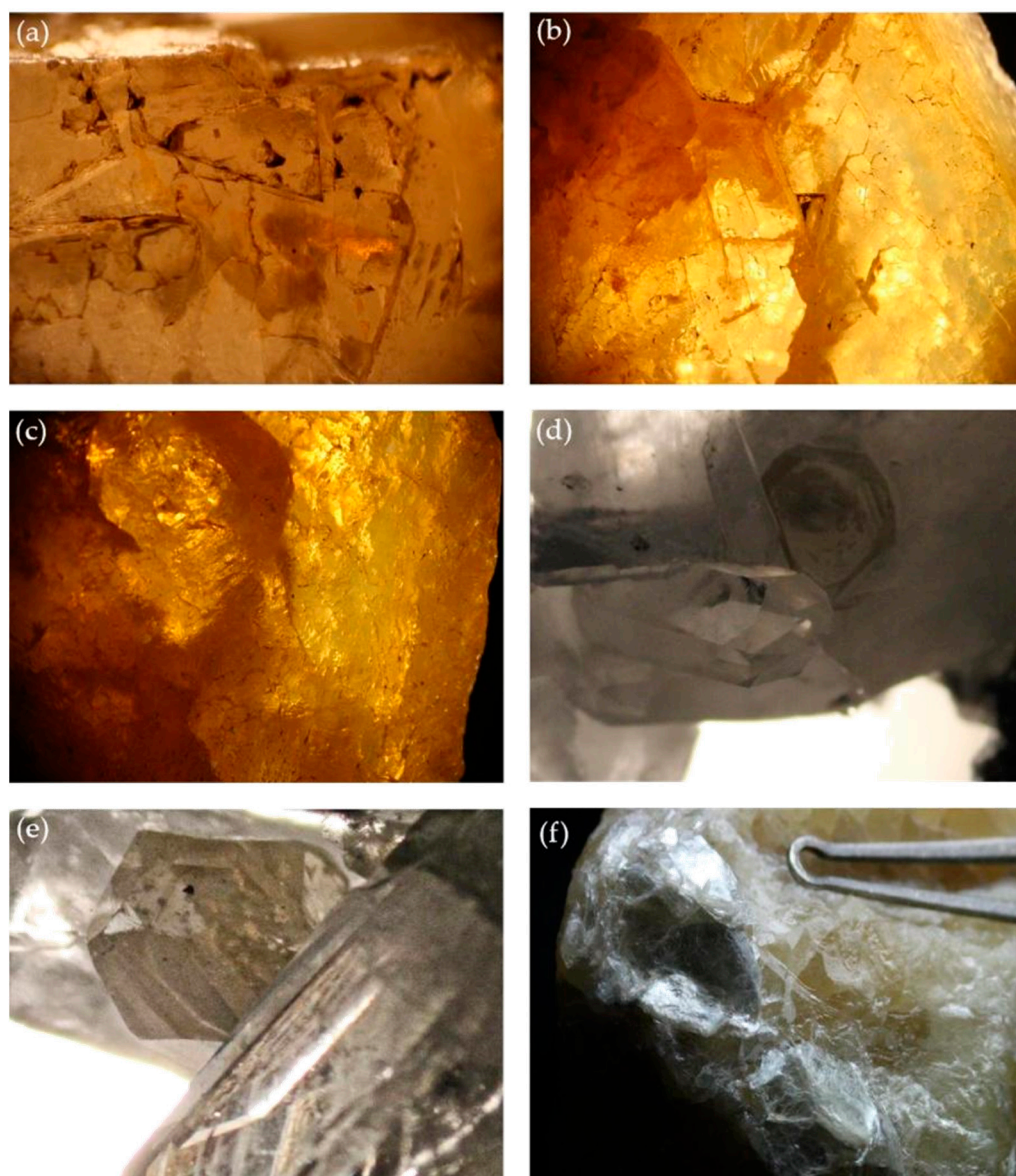


Figure 2. Observation of the internal characteristics by using a gemstone microscope. (a) Sample Sch-1 exhibited clear color bands. (b) Sample Sch-2 was relatively clean internally. (c) Sample Sch-3 was observed to be relatively clean internally. (d) Growth morphology was observed in sample Sch-4. (e) Sample Sch-4 revealed dark inclusions and a ring structure upon observation. (f) The naked eye observation of sample Sch-5 identified the presence of muscovite as an accessory mineral.

Table 1. Basic gemological mineralogical properties of scheelite from Xuebaoding.

Basic Properties	Sch-1	Sch-2	Sch-3	Sch-4	Sch-5
Color	Light yellow to yellow	Yellow	Yellow to orange	Nearly colorless	Light yellow
Relative density	6.07	6.14	6.11	5.81	6.13
Polarscope	Four bright and four dark	Four bright and four dark			
Zoomed in and observe	Color band	Clean	Clean	Dark inclusion and ring structure	Accessory mineral

All samples were found to exhibit significant fluorescence. The R–Sch samples with light yellow to orange tone showed no fluorescence at long wavelengths (L.W.), whereas medium to strong blue and white fluorescence was observed at short wavelengths (S.W.). In the A–Sch samples, white fluorescence was observed in Sch–4 (transparent and nearly colorless), while Sch–5 exhibited light blue fluorescence (translucent and light yellow tone) (refer to Table 2). According to previous research [1], it is known that as the color deepens, scheelite exhibits light yellow to white fluorescence. The observation of light blue fluorescence indicates the presence of 0.5 wt.% Mo in scheelite. In contrast, the observation of white fluorescence suggests that the Mo content exceeded 4.8 wt.%.

Table 2. Fluorescence characteristics and absorption spectra of scheelite from Xuebaoding.

Basic Properties	Sch–1	Sch–2	Sch–3	Sch–4	Sch–5
Fluorescence	L.W.	L.W.	L.W.	L.W.	L.W.
	no fluorescence	no fluorescence	no fluorescence	no fluorescence	no fluorescence
	S.W.	S.W.	S.W.	S.W.	S.W.
	medium blue to white fluorescence	strong blue to white fluorescence	strong blue to white fluorescence	white fluorescence	weak blue to white fluorescence
Grating spectroscopy	A weak absorption line in the yellow zone	Two weak absorption lines in the yellow zone	Two weak absorption lines in the yellow zone A weak absorption line in the green zone	A weak absorption line in the green zone	A weak absorption line in the yellow zone

4.1.2. Mineralogical Characteristics

The R–Sch samples with light yellow to orange tone were observed using a polarized light microscope. The granular structure was found to be evenly, uniformly distributed using single polarized light, with mineral defects and cracks evident and all resulting from the grinding of thin slices (Figure 3a,c,e). Additionally, R–Sch samples with light yellow to orange tone displayed interference colors of light blue, blue, and yellow when examined using orthogonal polarized light (Figure 3b,d,f). Single polarized light microscopy revealed that the A–Sch samples exhibited a uniformly distributed granular structure without noticeable discontinuities and includes muscovite as an accessory mineral (Figure 4a,c). Orthogonal polarized light microscopy allowed for observation of interference colors of blue and light blue in the A–Sch samples (Figure 4b,d).

Figure 5 illustrated the back scattered electron images of two groups of scheelite samples. The R–Sch samples with light yellow to orange tone demonstrate a uniform internal mineral distribution without any apparent discontinuities (Figure 5a–c). The A–Sch samples have been observed to contain scheelite, quartz, and some black masses. The black masses are due to the absence of minerals, and the adhesive used to fix the thin film turns black after carbon spraying. Interestingly, the black inclusions that resemble bubbles or gas liquid inclusions are actually bubbles within the glue (Figure 5d). Furthermore, observations of fluorite and calcite confirm that scheelite from Xuebaoding predominantly occupies tensile fractures of the marble between the Pankou and Pukouling granites (Figure 5e,f).

4.1.3. Crystallization Degree

The X-ray powder diffraction (XRD) patterns of the A–Sch samples are presented in Figure 6. Black minerals can be seen on the surface of sample Sch–4. In order to confirm which minerals they were, we conducted XRD tests on these minerals, and the results showed that the black minerals were found to consist of muscovite (M₁) $KAl_2(Si_3Al)O_{10}(OH)_2$, muscovite (M₂) $KAl_2(Si_3Al)O_{10}(OH,F)_2$, muscovite (M₃) $(K_{0.82}Na_{0.18})(Fe_{0.03}Al_{1.97})(AlSi_3)O_{10}(OH)_2$, and illite (I) $(K,H_3O)Al_2Si_3AlO_{10}(OH)_2$ (Figure 6a).

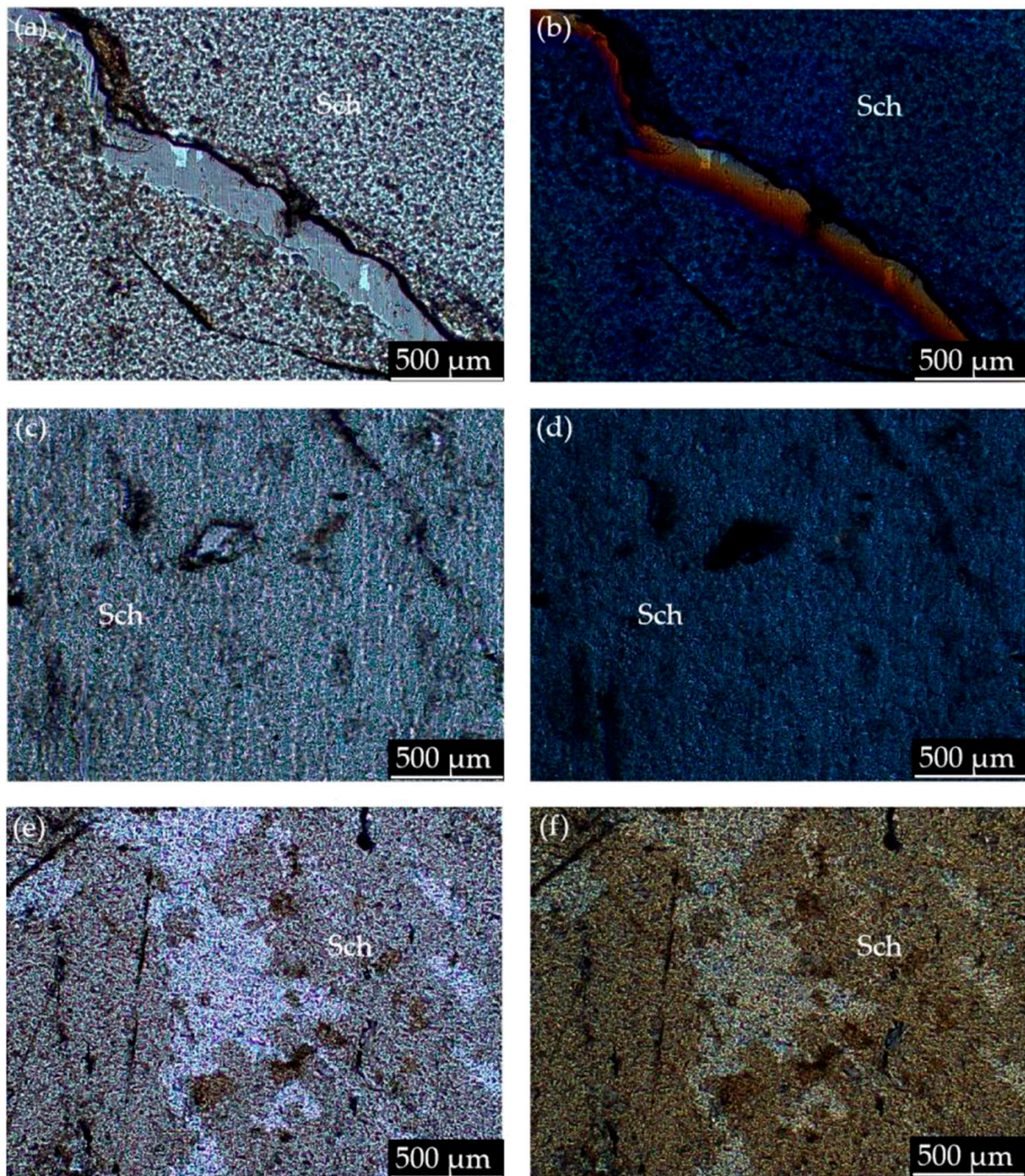


Figure 3. Observation of the R–Sch samples with light yellow to orange tones using a polarizing microscope. (a) Use of single polarized light and sample Sch–1 exhibited a uniformly distributed granular structure, with mineral deficiencies caused by grinding thin slices. (b) Employing orthogonal polarized light revealed an interference color of blue in sample Sch–1. (c) Sample Sch–2 displayed a uniformly distributed granular structure accompanied by cracks when observed using single polarized light. (d) Orthogonal polarized light showed an interference color of light blue in sample Sch–2. (e) Sample Sch–3 exhibited a uniformly distributed granular structure accompanied by cracks when observed using single polarized light. (f) Orthogonal polarized light revealed an interference color of yellow in sample Sch–3. Sch: scheelite.

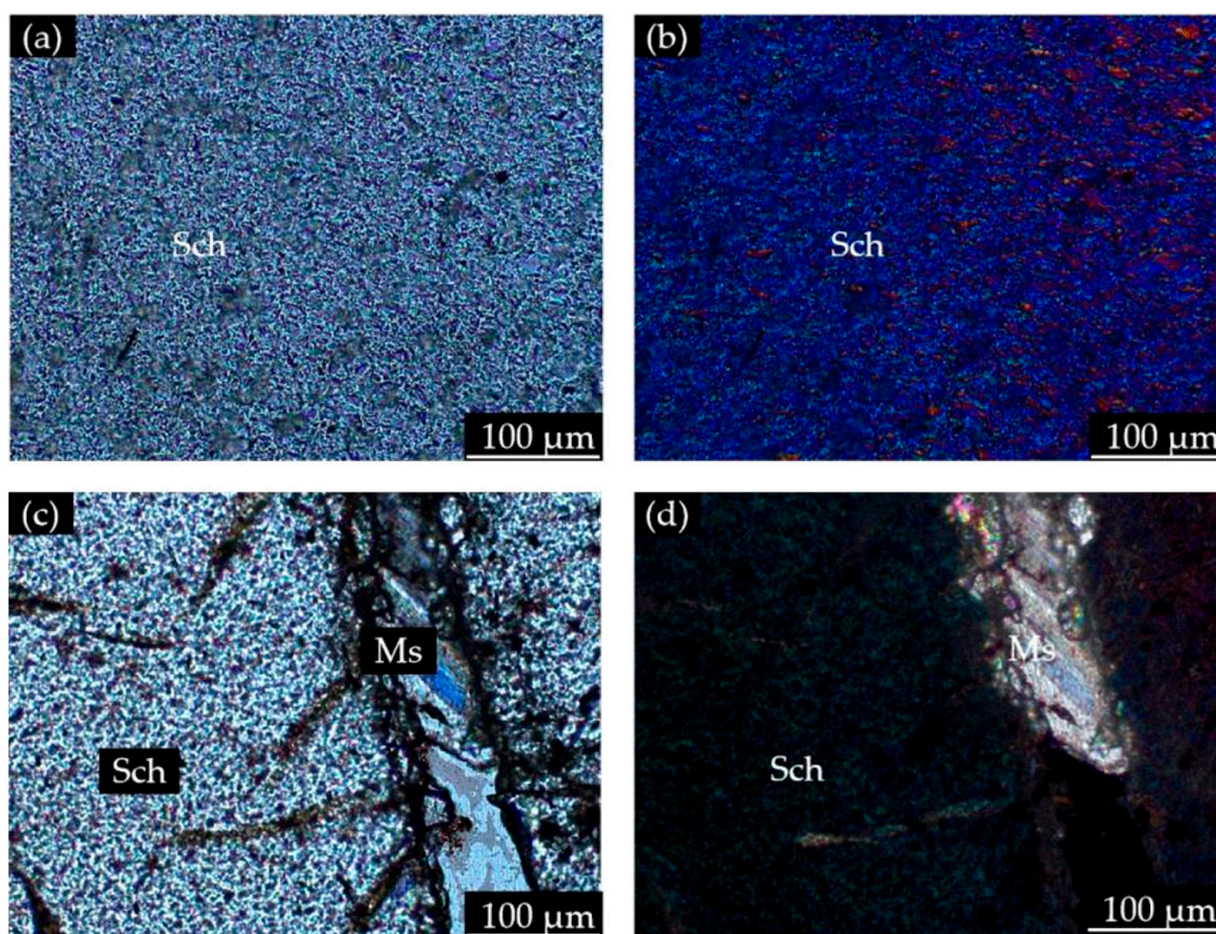


Figure 4. Observations of the A–Sch samples were made using the polarizing microscope. (a) Sample Sch–4 exhibited a uniform distribution of a granular structure without any noticeable discontinuities when observed with single polarized light. (b) Examining sample Sch–4 with orthogonal polarized light displayed interference colors of blue. (c) By utilizing single polarized light, sample Sch–5 showed a uniform distribution of granular structure without any apparent discontinuities, with muscovite identified as the accessory mineral. (d) Sample Sch–5 revealed interference colors of blue when viewed with orthogonal polarized light. Sch: scheelite Ms: muscovite.

The peaks indicated in Figure 6 are all characteristic peaks. However, the intensity of some peaks was too low and not considered to be analyzed as characteristic peaks in this study, therefore, they were not labeled. Characteristic strong spectral peaks of muscovite (M_1) with peak positions at 8.8° , 17.7° , 26.7° , and 45.2° can be seen in Figure 6a. Similarly, illite (I) exhibited characteristic strong spectral peaks at 8.8° and 45.2° , which can be detected in sample Sch–4. These peaks correspond to the crystal plane indices of (002), (004), (006), and (136). Additionally, muscovite (M_1) exhibited characteristic weak spectral peaks at 25.4° , 31.9° , 37.7° , 52.7° , 57.4° , 61.9° , 64.0° , 65.0° , and 69.3° , corresponded to crystal plane indices expressed as (-114) , (-116) , (133), (-139) , (313), (156), (316), (333), and (-1313) . Equally, muscovite (M_2) displayed characteristic weak spectral peaks at 19.8° , 23.8° , 35.8° , 37.7° , 42.3° , 52.8° , and 55.8° with crystal plane indices expressed as (-111) , (023), (-117) , (133), (135), (-139) and (139). Furthermore, the characteristic weak spectral peak of muscovite (M_3) were observed at 29.5° , 55.1° and 76.0° , corresponding to crystal plane indices of (025), (-314) , and (264). Illite (I) exhibited characteristic weak spectral peaks at 22.8° , 27.8° , 31.1° , and 35.0° , with crystal plane indices expressed as (-113) , (114), (115), and (131).

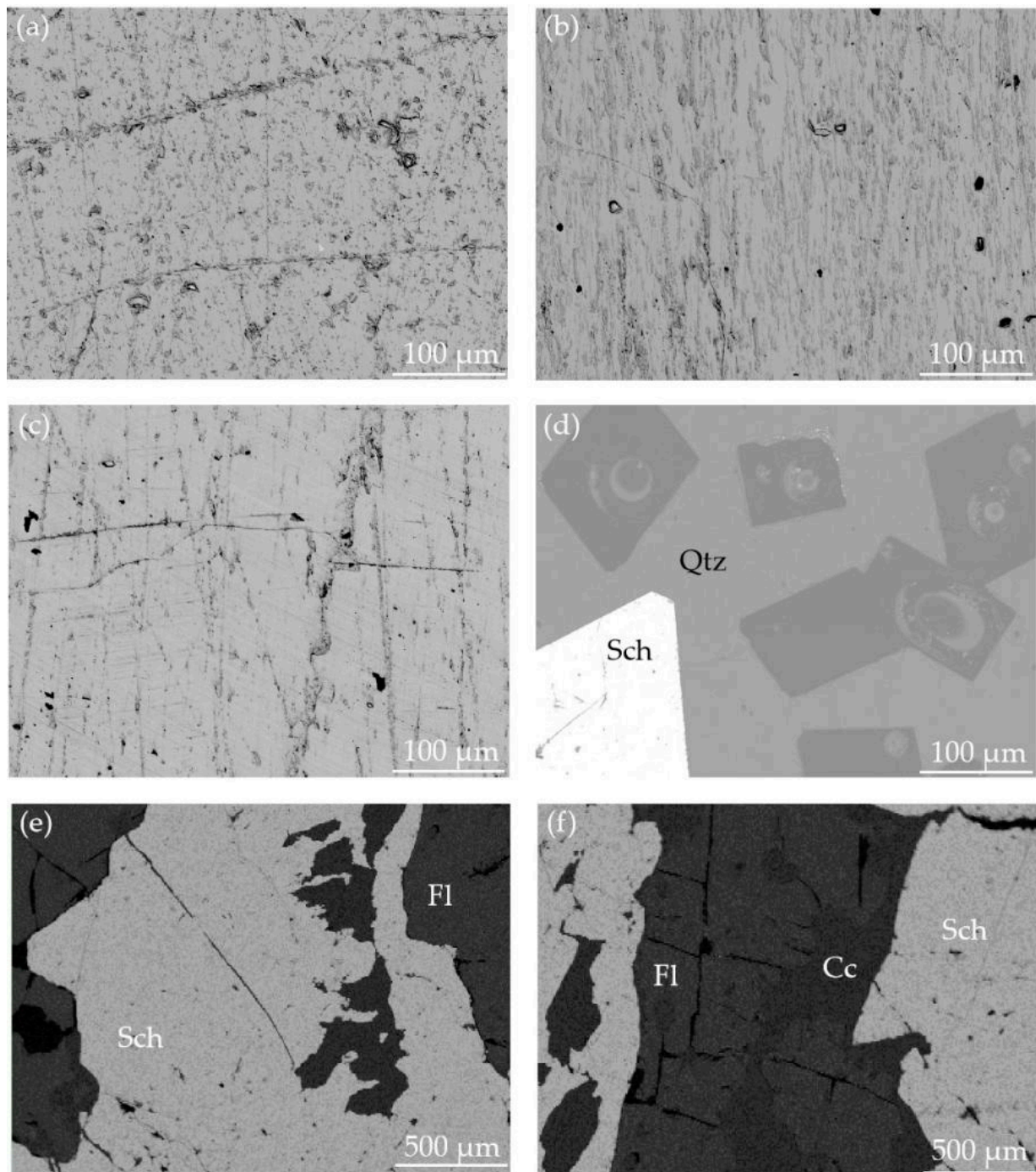


Figure 5. Back-scattered electron images of scheelite from Xuebaoding. (a) Sample Sch-1 exhibited a homogeneous internal mineral distribution without any noticeable interruptions. (b) Sample Sch-2 displayed a uniform internal mineral distribution devoid of any notable interruptions. (c) Sample Sch-3 demonstrated a homogeneous and uninterrupted internal mineral distribution. (d) In the case of sample Sch-4, accessory mineral quartz was observed, with the darker parts indicating potential mineral deficiencies. (e) Fluorite was detected within Sch-5. (f) Calcite was identified inside sample Sch-5. Sch: scheelite Qtz: quartz Fl: fluorite Cc: calcite.

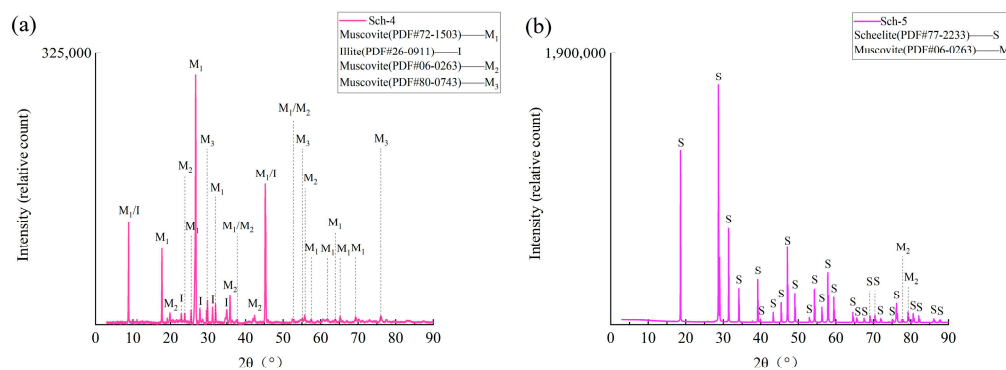


Figure 6. Detection of scheelite from Xuebaoding using X-ray powder diffraction grams. (a) Sch–4 exhibits muscovite and illite as accessory minerals. (b) Sch–5 shows muscovite as an accessory mineral.

The diffraction pattern of the sample Sch–5 (translucent and light yellow tone) (see Figure 6b) showed a remarkable similarity to the scheelite peak (PDF #77-2233) and contained trace amounts of muscovite (M_2) $KAl_2(Si_3Al)O_{10}(OH, F)_2$. Notably, the spectrum peak of scheelite (PDF #77-2233) utilized in study differed from previous investigations and aligned more closely with the sample employed herein. The characteristic strong spectral peaks of scheelite included 18.6° , 28.7° , 31.4° , 34.1° , 39.1° , 47.0° , 54.2° , 57.8° , and 59.4° , whereas the weaker spectral peaks encompassed 39.9° , 43.3° , 45.4° , 49.0° , 52.9° , 56.2° , 64.5° , 65.5° , 67.5° , 69.1° , 70.4° , 71.9° , 75.0° , 76.1° , 80.6° , 82.1° , 86.0° , and 87.5° all detected within sample Sch–5. Represented by the strong spectral peaks are the crystal plane indices (101), (112), (004), (200), (312), (211), (204), (116), (312), and (224). The crystal plane indices represented by weak spectral peaks are (114), (105), (123), (220), (301), (125), (321), (008), (305), (233), (127), (400), (141), (136), (404), (420), (228), and (129). Additionally, the characteristic spectral peak of muscovite (M_2) is observed at 77.8° and 79.2° , the crystal plane indices are expressed as (352) and (353). Since the main component of sample Sch–5 is scheelite, the crystallinity obtained by fitting the XRD pattern of sample Sch–5 using MDI Jade 6 software is considered to be the crystallinity of scheelite. Among the characteristic spectral peaks of scheelite, the crystallinity of each strong spectral peak were determined to be 85.48%, 77.93%, 91.12%, 96.71%, 95.73%, 92.58%, 96.64%, 95.03%, and 97.48%. Similarly, the crystallinity values of each spectral weak peak were found to be 99.67%, 99.01%, 98.06%, 97.09%, 99.48%, 98.48%, 98.96%, 99.46%, 99.52%, 99.27%, 99.25%, 99.52%, 99.61%, 98.06%, 99.02%, 99.24%, 99.52% and 99.75%. The higher crystallinity observed in each respective peak indicates a high degree of crystallinity within scheelite.

4.2. Geochemical Characteristics of Scheelite from Xuebaoding

4.2.1. Main Element Compositions

The R–Sch samples with light yellow to orange tone were subjected to analysis using an X-ray fluorescence spectrometer (XRF). The findings demonstrated the presence of WO_3 , CaO, and P_2O_5 , in the ranges of 79.16–80.86 wt.%, 17.17–17.60 wt.% and 0.75–1.64 wt.%, in all samples examined. Among them, the main constituents, WO_3 and CaO, constituted approximately 96 wt.% of the total mass, while also containing trace amounts of P_2O_5 , SO_3 , ReO_2 , and SrO, along with rare earth elements such as Y, Tm, etc. (see Table 3).

The data of two groups of scheelite samples detected by the electron microprobe showed that the main elements WO_3 and CaO, in the range of 79.92–80.95 wt.% and 19.37–19.68 wt.%, accounted for about 99 wt.% of the total mass, accompanied by trace amounts of SiO_2 , MnO, K_2O , Na_2O , MgO, and TiO_2 . Ideally, the mass ratios of WO_3 and CaO in $CaWO_4$ should be 80.56 wt.% and 19.44 wt.%, respectively. However, it was observed that the samples Sch–1 and Sch–2 exhibited a complete attainment or surpassing of the ideal values for WO_3 and CaO content, while the sample Sch–3 fell below the ideal value for WO_3 content alone. Furthermore, the associated mineral with scheelite samples

demonstrated WO_3 and CaO content either below or proximate to their respective ideal values (see Table 4).

Table 3. Chemical composition analysis of scheelite derived from Xuebaoding (wt.%).

Chemical Components	Sch-1	Sch-2	Sch-3
WO_3	80.86	79.16	79.47
CaO	17.43	17.60	17.17
P_2O_5	1.29	0.75	1.64
SO_3	0.37	0.40	-
Y_2O_3	0.05	-	0.04
ReO_2	-	1.32	1.57
Tm_2O_3	-	0.77	-
SrO	-	-	0.11
Total	100.0	100.0	100.0

Note: “-” indicates below detection limit or not detected.

Table 4. Main constituent composition of scheelite derived from Xuebaoding (wt.%).

Main Constituent	Sch-1	Sch-2	Sch-3	Sch-4	Sch-5
WO_3	80.62	80.95	79.92	80.73	80.28
CaO	19.68	19.61	19.54	19.37	19.68
SiO_2	0.23	0.25	-	-	0.25
MnO	0.01	0.02	0.01	-	0.07
K_2O	0.03	0.01	0.01	-	-
Na_2O	0.02	0.05	0.02	0.04	0.01
MgO	0.01	0.02	0.01	-	-
TiO_2	0.01	0.02	-	-	-
Total	100.61	100.93	99.50	100.14	100.29

Note: “-” indicates below detection limit or not detected.

4.2.2. In Situ Trace Element Characteristics

The two sample groups were analyzed at 30 points, and the trace element compositions of scheelite are shown in Table 5. In the R-Sch samples with light yellow to orange tone and the A-Sch sample Sch-5 (translucent and light yellow tone), the contents of trace elements Si, Sr, Fe, Y and Nb exceeded 10×10^{-6} , whereas the contents of trace elements Mg, Mn, Ge and Pb were below 10×10^{-6} but above 1×10^{-6} . However, the contents of trace elements Si, Sr, Fe, and Y in the A-Sch sample Sch-4 (transparency and nearly colorless) exceeded 10×10^{-6} , while the contents of trace elements Li, P, Nb, and Mo were below 10×10^{-6} but above 1×10^{-6} . Among the trace elements mentioned above, Sr and Nb could exhibit isomorphism with Ca^{2+} , while Nb and Mo could exhibit isomorphism with W^{6+} . The A-Sch sample Sch-4 (transparent and nearly colorless) contained the most Mo, and a ring structure was visible (Figure 3e). Due to the ubiquitous presence of Mo elements in scheelite, approximately 25 wt.% of W within the mineral lattice was substituted by Mo in isomorphism. As a result, scheelite containing Mo was presented in two different particle forms, light and dark. It often manifests as light-colored scheelite surrounded by dark-colored scheelite, displaying an uneven ring distribution. Consequently, there exists a significant inverse relationship between the content of the W and Mo elements [16]. The scheelite from Xuebaoding region exhibits a relatively high abundance of the lithophile element Sr, with an average value of 166.93×10^{-6} and content ranging from 13.58 to 541.99×10^{-6} . The ratios of Rb/Sr, Nb/Ta, and Zr/Hf were within the ranges of 0 – 0.02×10^{-6} , 21.70 – 76.37×10^{-6} , and 8 – 63×10^{-6} , respectively, with mean values of approximately 0.01×10^{-6} , 48.36×10^{-6} , and 26.78×10^{-6} . Of particular note is the remarkably low Rb/Sr ratio which may be due to the isomorphism of Sr and Ca^{2+} . Furthermore, the lower Rb/Sr and Nb/Ta ratios may indicate that the ore-forming materials of scheelite exhibit characteristics indicative of a shell source.

Table 5. Trace element composition of scheelite from Xuebaoding ($\times 10^{-6}$).

Trace Element	Sch-1	Sch-2	Sch-3	Sch-4	Sch-5	Average Value
Si	922.30	569.87	701.26	619.13	588.76	680.26
P	3.54	0.10	1.14	1.38	0.42	1.32
As	0.51	0.60	0.47	0.31	0.26	0.43
Li	1.86	0.34	0.21	8.52	0.41	2.27
Be	-	-	0.28	0.00	0.17	0.15
Na	3.17	1.90	8.53	0.51	0.94	3.01
Mg	2.14	3.67	1.30	0.49	3.49	2.22
K	0.23	0.46	0.25	0.19	0.26	0.28
Ga	0.84	0.91	0.89	0.04	0.60	0.66
Ge	2.81	3.44	2.60	0.24	1.75	2.17
Rb	0.25	0.21	0.30	0.05	0.29	0.22
Sr	42.17	15.29	221.63	541.99	13.58	166.93
Sn	0.03	0.04	0.03	0.01	0.02	0.03
Pb	3.52	3.83	2.17	0.78	3.36	2.73
Sc	0.01	0.02	0.00	0.02	0.01	0.01
Ti	0.04	0.20	0.01	0.03	0.03	0.06
V	0.01	0.00	0.00	0.01	0.01	0.01
Cr	0.37	0.45	0.21	0.30	0.51	0.37
Mn	5.17	11.27	6.17	0.17	9.44	6.44
Fe	20.74	21.26	21.51	19.91	20.42	20.77
Co	0.03	0.02	0.02	0.02	0.02	0.02
Ni	0.05	0.04	0.05	0.07	0.06	0.05
Y	58.76	26.19	62.87	13.92	20.86	36.52
Zr	0.56	0.67	0.38	0.47	0.63	0.54
Nb	47.98	35.13	36.67	1.91	18.26	27.99
Mo	0.46	0.69	0.45	4.36	0.81	1.35
W	147,244.50	146,973.75	147,473.88	138,478.00	139,973.43	144,028.71
Hf	0.07	0.06	0.08	0.01	0.01	0.05
Ta	0.94	0.46	1.69	0.06	0.30	0.69
Th	0.10	0.21	0.02	0.93	0.87	0.43
U	0.09	0.25	0.03	0.42	0.91	0.34
Rb/Sr	0.01	0.01	0.00	0.00	0.02	0.01
Nb/Ta	51.04	76.37	21.70	31.83	60.87	48.36
Zr/Hf	8.00	11.17	4.75	47.00	63.00	26.78

Note: “-” indicates below detection limit or not detected.

Chondrite-normalized REE patterns for the scheelite from Xuebaoding are depicted in Figure 7, with the chondrite-normalized values utilized were obtained by previous researchers [17]. As can be observed in Figure 7a, the curve of the R–Sch samples with light yellow to orange tone evidently has a right-dipping trend and the Eu element depletion. Similarly, the A–Sch samples exhibits a clear right-dipping curve, also indicating Eu depletion (see Figure 7b), as can be seen from Table 6, with the characteristics of REE content. The total rare earth elements (Σ REE) of scheelite from Xuebaoding range from 30.32 to 188.74×10^{-6} , with an average value of 124.66×10^{-6} , demonstrating a low REE content and a wide range of variation. Moreover, the LREE/HREE content ranges from 2.61 – 3.22×10^{-6} , suggesting that the REE composition is more enriched in LREE than in HREE. Notably, Eu exhibits significant negative anomalies, with the δ Eu range from 0.48 to 0.88×10^{-6} . However, Ce exhibits insignificant anomalies, with the δ Ce range from 0.89 to 1.01×10^{-6} . The results indicate higher elemental contents of Nd and Sm in the R–Sch samples with light yellow to orange tone, while relatively low content was found in the A–Sch sample Sch-4 (transparent and nearly colorless), higher content was present in sample Sch-5 (translucency and light yellow tone). High contents of rare earth elements such as La, Ce, Nd, Sm, Gd, Dy, and Y were detected. Scheelite crystallizes in the tetragonal system and elements such as Na, Sr, Y, Pb and REE can substitute for Ca^{2+} in the scheelite structure [18]. In addition, Mo^{6+} and Nb^{5+} can also substitute for W^{6+} in the tetrahedral WO_4^{2-} sites of scheelite [19].

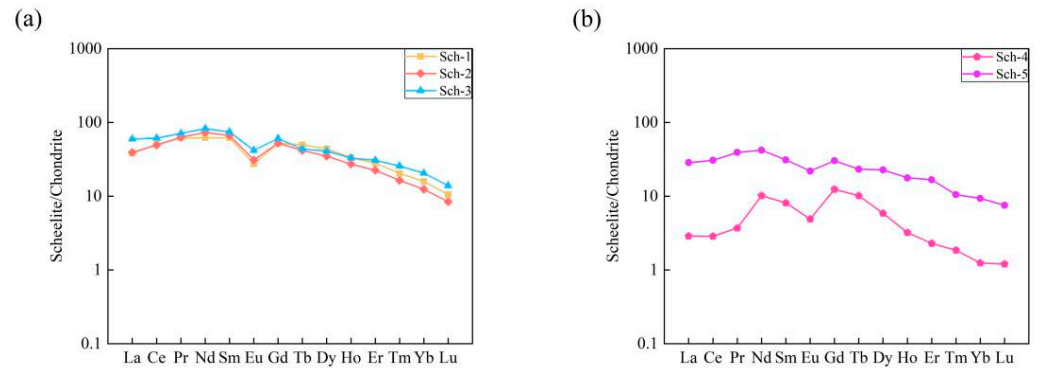


Figure 7. Chondrite-normalized REE patterns for the scheelite from Xuebaoding. (a) The R–Sch samples with light yellow to orange tones exhibit consistent curves and significant Eu elemental depletion. (b) In the A–Sch samples, a significant difference in content between the two samples can be seen, with the sample Sch–4 (transparent and nearly colorless) having a lower content.

Table 6. Rare earth element composition of scheelite from Xuebaoding ($\times 10^{-6}$).

Rare Earth Element	Sch–1	Sch–2	Sch–3	Sch–4	Sch–5	Average Value
La	11.89	12.13	18.53	1.98	8.83	10.67
Ce	40.58	39.85	49.33	10.05	24.75	32.91
Pr	7.48	7.68	8.64	2.64	4.78	6.24
Nd	37.11	43.90	49.36	6.09	25.23	32.34
Sm	12.08	12.94	14.50	1.58	6.05	9.43
Eu	2.01	2.27	3.08	0.36	1.61	1.87
Gd	13.56	13.70	15.69	3.21	7.81	10.79
Tb	2.36	1.97	2.06	0.48	1.10	1.59
Dy	14.09	11.20	13.17	1.89	7.32	9.53
Ho	2.39	1.95	2.37	0.42	1.27	1.68
Er	5.87	4.71	6.43	0.93	3.51	4.29
Tm	0.66	0.53	0.83	0.11	0.34	0.49
Yb	3.31	2.59	4.29	0.54	1.95	2.54
Lu	0.35	0.28	0.46	0.04	0.25	0.28
Y	58.76	26.19	62.87	13.92	20.86	36.52
Σ RFF + Y	212.50	181.89	251.61	44.24	115.66	161.18
Σ REE	153.74	155.7	188.74	30.32	94.80	124.66
LREE	111.15	118.77	143.44	22.70	71.25	93.46
HREE	42.59	36.93	45.30	7.62	23.55	31.20
LREE/HREE	2.61	3.22	3.17	2.98	3.03	3.00
(La/Yb) _N	2.42	3.16	2.91	2.47	3.05	2.80
(La/Sm) _N	0.62	0.59	0.80	0.79	0.92	0.74
(Gd/Yb) _N	3.31	4.22	2.95	4.80	2.04	3.46
δ Eu	0.48	0.52	0.62	0.48	0.88	0.59
δ Ce	1.01	0.97	0.93	0.89	0.91	0.94

4.2.3. In Situ Sr-Nd Isotope Characteristics

Sr, Sm, and Nd elemental and isotopic characteristics of scheelite from Xuebaoding were analyzed, and the results are presented in Table 7. At the same times, multiple samples were tested at 15 different points. Finally, the findings indicated that the Sr elemental content of scheelite ranges from 13.58 to 541.99 $\times 10^{-6}$, while the variation

range of $^{87}\text{Rb}/^{86}\text{Sr}$ and $^{87}\text{Sr}/^{86}\text{Sr}$ values was observed to be between 0.00003 to 0.00149 and 0.71103 to 0.75407, respectively. Furthermore, the Sm elemental content ranged from 1.58 to 14.5×10^{-6} and Nd element content ranged from 6.09 to 49.36×10^{-6} in scheelite samples obtained from the Xuebaoding region. Similarly, the range of $^{147}\text{Sm}/^{144}\text{Nd}$ and $^{143}\text{Nd}/^{144}\text{Nd}$ values varied from 0.1690 to 0.4042 and from 0.51147 to 0.54555, respectively. However, the Sm/Nd ratio of scheelite from Xuebaoding ranged between 0.24 and 0.33. The application of the Sm-Nd isotopic system for scheelite dating has been successfully demonstrated by previous research [20,21].

Table 7. Sr-Nd Isotopes of scheelite from Xuebaoding.

Isotope	Sch-1	Sch-2	Sch-3	Sch-4	Sch-5
Sr/ 10^{-6}	42.17	15.29	221.63	541.99	13.58
Sm/ 10^{-6}	12.08	12.94	14.50	1.58	6.05
Nd/ 10^{-6}	37.11	43.9	49.36	6.09	25.23
Sm/Nd	0.33	0.29	0.29	0.26	0.24
$^{87}\text{Rb}/^{86}\text{Sr}$	0.00097	0.00149	0.00019	0.00003	0.00148
$^{87}\text{Sr}/^{86}\text{Sr}$	0.71789	0.71920	0.71103	0.75407	0.71477
$\pm 2\sigma$	0.0006	0.0010	0.0001	0.0001	0.0001
$^{147}\text{Sm}/^{144}\text{Nd}$	0.2092	0.2307	0.1690	0.4042	0.1614
	0.2189	0.2059	0.1778		
$\pm 2\sigma$	0.0005	0.0011	0.0005	0.0239	0.0004
	0.51199				
$^{143}\text{Nd}/^{144}\text{Nd}$	0.51147	0.51196	0.51168	0.54555	0.51177
	0.51190	0.51181	0.51199		
$\pm 2\sigma$	0.0003	0.0004	0.0004	0.0214	0.0005
	-12.64				
$\epsilon_{\text{Nd}}(0)$	-22.78	-13.23	-18.69	641.95	-16.93
	-14.40	-16.15	-12.64		
	-10.77				
$\epsilon_{\text{Nd}}(t)$	-10.54	-10.27	-11.71	-6.21	-11.89
	-10.47	-10.85	-11.51		

Both groups of tested samples exhibit a linear distribution trend, however, only the R-Sch samples with light yellow to orange tones and the A-Sch sample Sch-5 could demonstrate a good straight line of fit. The Isoplot program [22] was used for analyzing Sm-Nd isotopic ages, with a decay constant value of $\lambda = 6.54 \times 10^{-12} \text{ a}^{-1}$ for ^{147}Sm utilized in the calculation. Chondrite Uniform Reservoir (CHUR) values of 0.1967 for $^{147}\text{Sm}/^{144}\text{Nd}$ and 0.512637 for $^{143}\text{Nd}/^{144}\text{Nd}$ were adopted [23]. Thus, the results indicate an isochronal age of $(183 \pm 8.6) \text{ Ma}$ ($n = 8$, MSWD = 1.1) with an initial ratio of $^{143}\text{Nd}/^{144}\text{Nd}$ as (0.5116 ± 0.0012) for scheelite from Xuebaoding, all within the error range (see Figure 8). According to the ICS international chronostratigraphic chart [24], the age of scheelite can be inferred as dating from the Toarcian stage in the Lower Jurassic Epoch. During the process, the $\epsilon_{\text{Nd}}(t)$ and the $\epsilon_{\text{Nd}}(0)$ values were calculated for scheelite from Xuebaoding at $t = 183 \text{ Ma}$, yielding ranges of -10.27 to -11.89 (average: -11.00), and -12.64 to -22.78 (average: -15.93), respectively. Because of the extremely low measured Rb element content amounts in scheelite, all below 1×10^{-6} , the contribution of ^{87}Sr from the decay of ^{87}Rb can be considered negligible. Based on this, the measured values of $(^{87}\text{Sr}/^{86}\text{Sr})_0$ can be replaced with $^{87}\text{Sr}/^{86}\text{Sr}$ to elucidate the provenance of ore-forming materials.

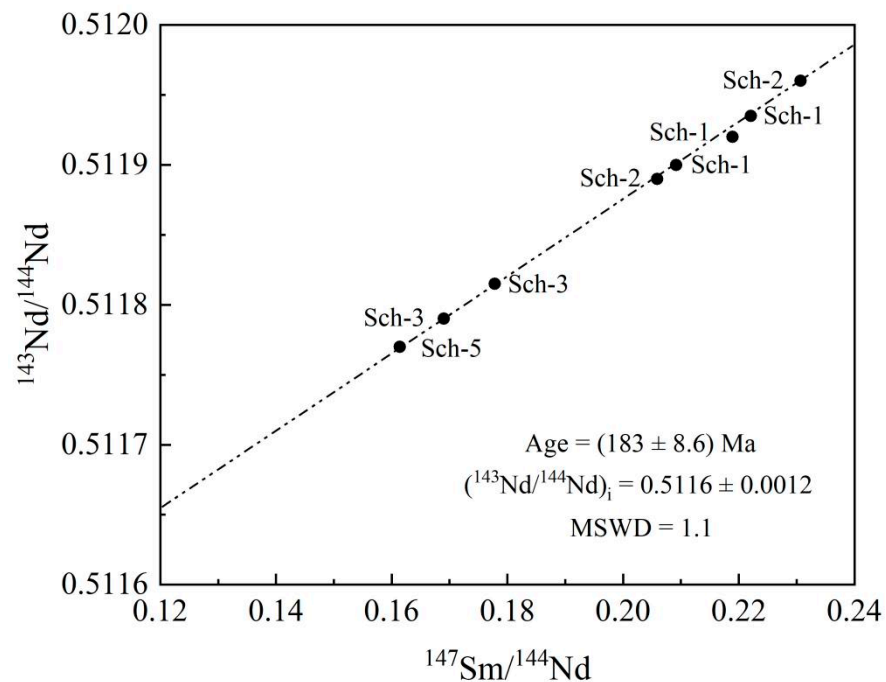


Figure 8. An Sm-Nd isotope isochronal chart of scheelite from Xuebaoding, indicating a metallogenic age of 183 Ma, formed in the Lower Jurassic Epoch.

5. Discussion

5.1. Rare-Earth Patterns of Scheelite from Xuebaoding

The rare-earth patterns of scheelite from the Xuebaoding W-Sn-Be deposit, as studied in this paper, were basically consistent with previous researchers [25]. A relatively smooth transition pattern was exhibited, with a slight enrichment of LREEs and a minor loss of HREEs. There were no significant anomalies observed for Ce, while an evident moderately negative anomaly was observed for Eu. However, it should be noted that the total content of rare earths was comparatively low compared to previous studies. The moderately negative anomalies exhibited by Eu elements ($\delta \text{Eu} = 0.48\text{--}0.88 \times 10^{-6}$, average: 0.59×10^{-6}) were similar to those found in the oxide stage scheelite from the Donggushan tungsten deposit in Anhui Province ($\delta \text{Eu} = 0.30\text{--}0.68 \times 10^{-6}$, average: 0.51×10^{-6}). Additionally, the rare-earth patterns displayed clear enrichment in LREEs and deficiency in HREEs [26]. They were clearly different from scheelite in other regions, such as the three generations of scheelite from Guilin Zhengfu Molybdenum in the Jiangnan tungsten belt ($\delta \text{Eu} = 0.08\text{--}0.99 \times 10^{-6}$, $0.09\text{--}0.26 \times 10^{-6}$, and $0.11\text{--}0.36 \times 10^{-6}$), scheelite from Zhaishang gold mine in the West Qinling Mountains ($\delta \text{Eu} = 0.75\text{--}1 \times 10^{-6}$), scheelite from the Xianggou gold and tungsten mines in the South Qinling Mountains ($\delta \text{Eu} = 0.61\text{--}0.83 \times 10^{-6}$, average: 0.72×10^{-6}), and scheelite from the Baojinshan mine in Hunan Province ($\delta \text{Eu} = 0.87\text{--}1.44 \times 10^{-6}$) [27–30]. Thus, the rare-earth patterns of scheelite from Xuebaoding exhibit a difference from the conventional MREE enriched type and instead display a flat type without MREE enrichment, accompanied by negative Eu anomalies. Based on this, the tetrad effect in the rare-earth patterns is characterized by a gradual decrease in LREEs and HREEs [25]. Of course, the salinity of the ore-forming fluid in the Xuebaoding beryl scheelite deposit is classified as low salinity within the NaCl-CO₂-H₂O system, with scheelite exhibiting a predominant salinity range between 3% and 6% (NaCl) [12]. However, both sample groups utilized in this study lacked sodium minerals, displaying a lower chemical composition content of Na₂O ranging from 0.01 to 0.05%, along with the trace element Na at levels of $0.51\text{--}8.53 \times 10^{-6}$. Therefore, the above findings suggest that the scheelite from Xuebaoding was formed in a low-sodium environment. Moreover, the influencing factor of rare-earth patterns is the partition coefficient of rare earths in the hydrothermal fluid rather than crystal chemistry.

The tetrad effect of rare earths refers to the demarcation point represented by Nd/Pm, Gd, Ho/Er, where every four rare earths constitute a distinct group; that is La-Ce-Pr-Nd, Pm-Sm-Eu-Gd, Gd-Tb-Dy-Ho, and Er-Tm-Yb-Lu. According to the arrangement of atomic numbers, specific physical and chemical properties or their natural composition gives rise to four groups of convex or concave curves. The convex curve represents the M type rare earth tetrad effects, while the concave curve corresponds to the W-type rare earth tetrad effects [31]. By quantitatively identifying the rare earth tetrad patterns of scheelite from Xuebaoding as either M type or W type, based on the parameters proposed by Irber [32] and Monecke et al., [33] we utilized the central elements (Ce, Pr or Tb, Dy) of each quaternary subgroup from both sample groups. Using the prescribed methodology, the normalized values of the chondrites (Ce_N , Pr_N or Tb_N , Dy_N) can be computed, along with the interpolation ratio (Ce_N/Ce^* , Pr_N/Pr^*) for the initial elements (La, Gd) and final elements' (Nd, Ho) lines within each of the four subgroups. As a result, the M-type rare earth tetrad types exhibit a ratio greater than one and a convex curve, whereas the W type rare earth tetrad types demonstrate the opposite [34]. The intensities were measured using Irber and Monecke's method to calculate T_1 , T_3 , t_1 , t_3 , and $TE_{1,3}$, and the corresponding calculation results are shown in Table 8. From the obvious tetrad effect of $TE_{1,3} > 1.10$, the samples Sch-1 and Sch-4 exhibit the rare earth tetrad effects is clearly within the two groups of scheelite samples, while samples Sch-2, Sch-3, and Sch-5 do not display a pronounced effect. Although the method can be applied to granite, the scheelite from Xuebaoding mainly occurs in the tensile fractures of marble between the Pankou and Pukouling granite, thus the method is applicable.

Table 8. The M and W type four group effect parameters of scheelite from Xuebaoding.

Four Group Effect	Sch-1	Sch-2	Sch-3	Sch-4	Sch-5
Ce_N/Ce^*	1.12	1.02	0.92	1.67	0.94
Pr_N/Pr^*	1.16	1.06	0.96	2.49	1.06
Tb_N/Tb^*	1.11	0.99	0.88	1.05	0.92
Dy_N/Dy^*	1.13	1.03	1.01	0.78	1.08
Tm_N/Tm^*	1.01	1.01	1.09	1.18	0.82
Yb_N/Yb^*	1.09	1.06	1.14	1.39	0.95
T_1	0.18	0.06	0.07	1.56	0.07
T_3	0.13	0.03	0.06	0.25	0.15
t_1	1.14	1.04	0.94	2.04	1.00
t_3	1.12	1.01	0.94	0.91	0.99
$TE_{1,3}$	1.13	1.02	0.94	1.36	1.00

Note: $Ce^* = La_N^{2/3} \times Nd_N^{1/3}$; $Pr^* = La_N^{1/3} \times Nd_N^{2/3}$; $Tb^* = Gb_N^{2/3} \times Ho_N^{1/3}$; $Dy^* = Gb_N^{1/3} \times Ho_N^{2/3}$; $Tm^* = Er_N^{2/3} \times Lu_N^{1/3}$; $Yb^* = Er_N^{1/3} \times Lu_N^{2/3}$ [34]. $TE_{1,3}$ is defined as the degree of tetrad effect.

5.2. The Metallogenic Age of Scheelite from Xuebaoding

The interior of the scheelite crystals in both sample groups exhibited uniform mineral composition and no growth discontinuities. Meanwhile, Sm-Nd isotope dating showed represent a metallogenic age of 183 Ma for the formation of scheelite, which was occurring during the Lower Jurassic Epoch, which aligns well with previous studies [25]. In addition, the $^{40}Ar/^{39}Ar$ fast neutron activation dating of quartz was employed to determine a metallogenic age of 186 Ma for the Xuebaoding deposit, which belongs to the early Yanshan period. Moreover, the mineral crystallization solution was formed during the magmatic period (224 Ma), while the hydrothermal activity associated with mineralization primarily took place after this period (186–192 Ma) [12]. However, due to limitations in using only quartz for determining metallogenic age and considering that the P-T conditions for quartz formation span a wide range, the direct utilization of quartz for the age of the Xuebaoding deposit is not feasible. Although both sample groups used in the article are

from Xuebaoding, but do not belong to the same vein and lack accessory minerals such as cassiterite, beryl, and other minerals, so they only represent the metallogenic age of scheelite. Nevertheless, the main metallogenic age of the Xuebaoding W-Sn-Be rare metal deposit is represented by a metallogenic age of 182 Ma observed in scheelite deposits within the second belt of Xuebaoding vein due to its close symbiotic relationship with minerals like cassiterite and beryl [25].

5.3. Genesis Types of Scheelite from Xuebaoding

According to previous research, the Xuebaoding W-Sn-Be deposit may represent a novel type of deposit related to A type granite [25]. Of course, four important indicators of A type granite have been discovered. Firstly, the presence of enriched Si, Na, K elements and the absence of Ca, Mg and Al elements are present in the rocks. Secondly, there are high ratios of $(K_2O + Na_2O)/Al_2O_3$, FeO/MgO and Ga/Al values. Thirdly, enrichment in high-field-strength elements such as Rb, Th, Nb, Ta, Zr, Hf, Ga, Y is observed while Sr, Ba, Cr, Co, Ni, V, Eu, Ti and P elements are barren. Fourthly, the right dipping seagull type REE distribution pattern and significant negative Eu anomalies are evident [35]. Based on the study, the primitive mantle standardized spider graph of trace elements (see Figure 9) in two groups of sample scheelite from the Xuebaoding demonstrates that the scheelite is enriched in elements such as La, Nd, and Y, while exhibiting a significant lack of high-field-strength elements including P, Zr, and Ti, as well as large ion lithophile elements like K and Ba. In addition, the range of values for $10^4 \times Ga/Al$ values between 3.50 and 5.67, which is notably higher than that of the I type (average: 2.1) and S type (average: 2.28) granite, indicate a consistency with A-type granite (>2.6) [36]. However, on the graphs of Nb, Ce, Zr, $Y-10^4 \times Ga/Al$ (see Figure 10), both sample groups are classified within the A type region. In summary, the genesis type of scheelite from Xuebaoding is A-type granite, which serves as the ore-bearing host rock of scheelite, which can be mutually confirmed with the tensile fractures of marble mainly occurring between the Pankou and Pukouling granites.

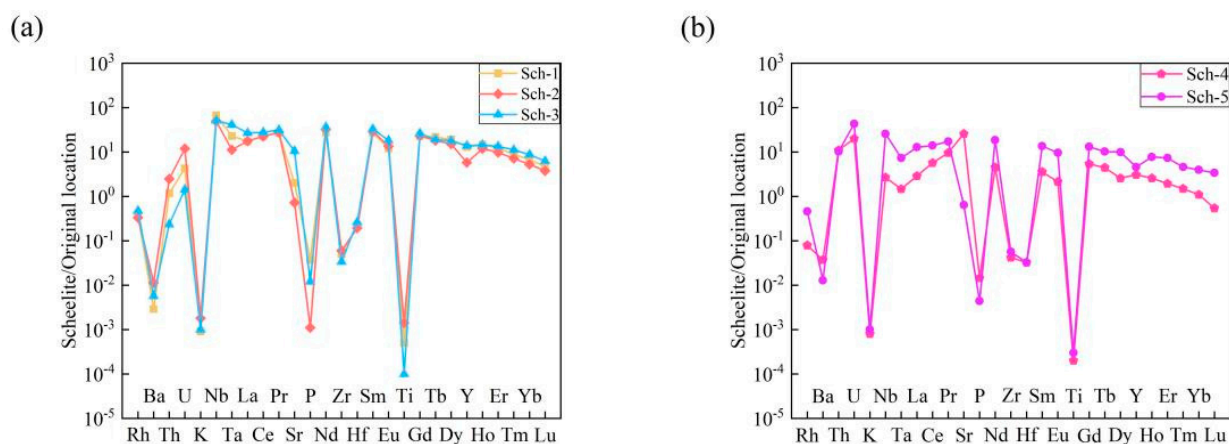


Figure 9. Primitive mantles standardized the spider graph of trace elements in scheelite from Xuebaoding. (a) In R–Sch samples with light yellow to orange tone, the curve fluctuations exhibit relatively consistent, characterized by barren high-field-strength elements such as P, Zr, Ti, and large ion lithophile elements like K and Ba. (b) In the A–Sch samples, both samples demonstrate similar contents of barren high-field-strength elements including P, Zr, and Ti.

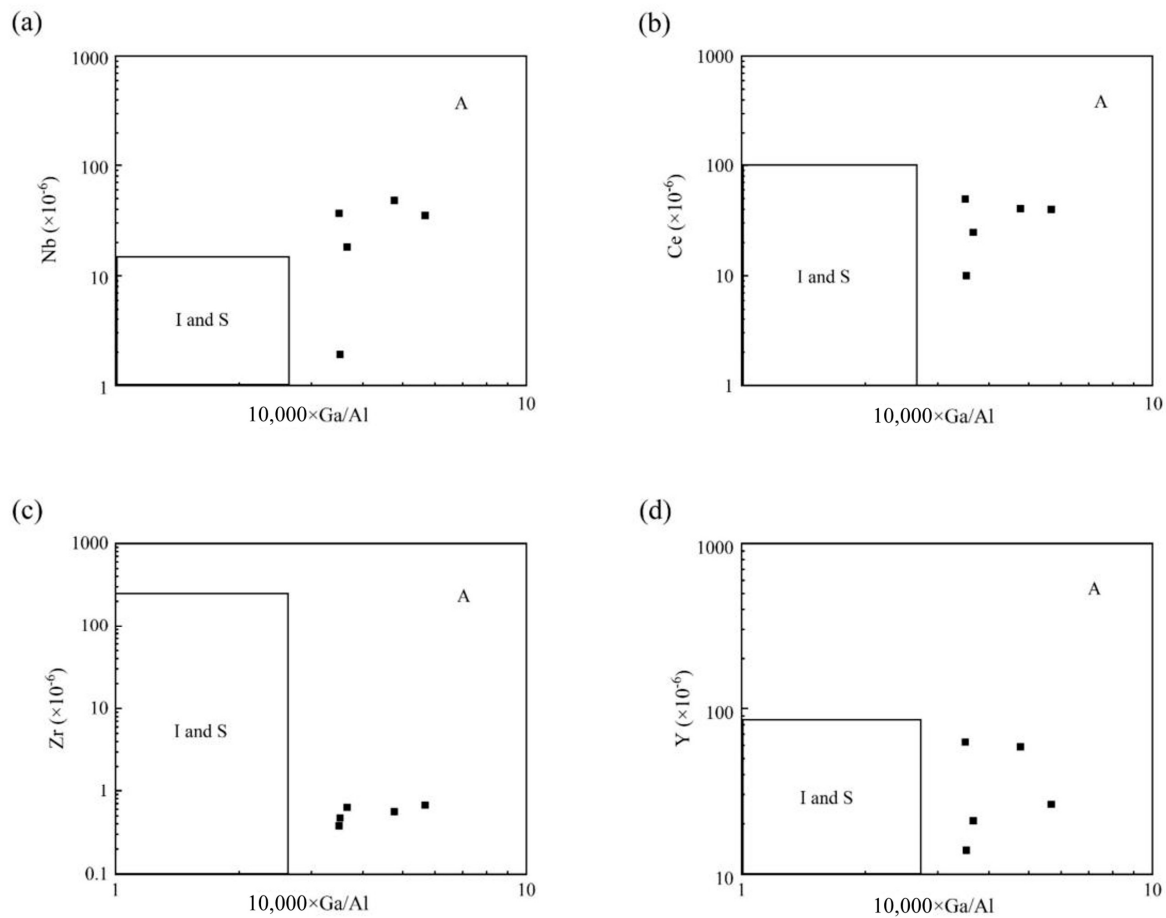


Figure 10. Diagram of Nb, Ce, Zr, $Y \cdot 10^4 \times Ga/Al$ in scheelite from Xuebaoding according to previous studies [36]. (a) The diagram of Nb– $10^4 \times Ga/Al$ in two groups of scheelite samples, it can be seen that both fall into the A region but are dispersed in distribution. (b) Diagram of Ce– $10^4 \times Ga/Al$ in two groups of scheelite samples shows that the samples all fall into the A region and are more dispersed. (c) As shown in the diagram of Zr– $10^4 \times Ga/Al$ in two groups of scheelite samples, both fall into the A region and the distribution is concentrated. (d) $Y \cdot 10^4 \times Ga/Al$ diagram of two groups of scheelite samples both fall into the A region, with a relatively dispersed distribution.

5.4. The Source of Ore-Forming Materials of Scheelite from Xuebaoding

The Sr-Nd isotopes in scheelite is very effective indexes to confirm the source of the ore-forming minerals [37]. The $\epsilon_{Nd}(t)$ values of scheelite from Xuebaoding range from -10.27 to -11.89 , while the $(^{87}Sr/^{86}Sr)_0$ values span between 0.71103 and 0.71920, with an average value of 0.71512. However, the average $^{87}Sr/^{86}Sr$ ratio of crustal derived magma is typically 0.719, while magma with ratio ranging from 0.706 to 0.719 originates from the source region where crust and mantle mix. At the same time, the value of $\epsilon_{Nd}(t)$ is bounded by 0, with positive values indicating magma derived from the depleted mantle and negative values representing the magma sourced crust or enriched mantle [38]. From the range of endpoint values in the $(^{87}Sr/^{86}Sr)_0 - \epsilon_{Nd}(t)$ relationship diagram, it can be found that the scheelite from Xuebaoding mainly originates from the upper crust and a subset of samples fall within the younger crust region (Figure 11). Samples Sch–1, Sch–2, and Sch–3 are located in the upper crust, sample Sch–5 is located in the younger crust, and sample Sch–4 is not within the range shown in the figure.

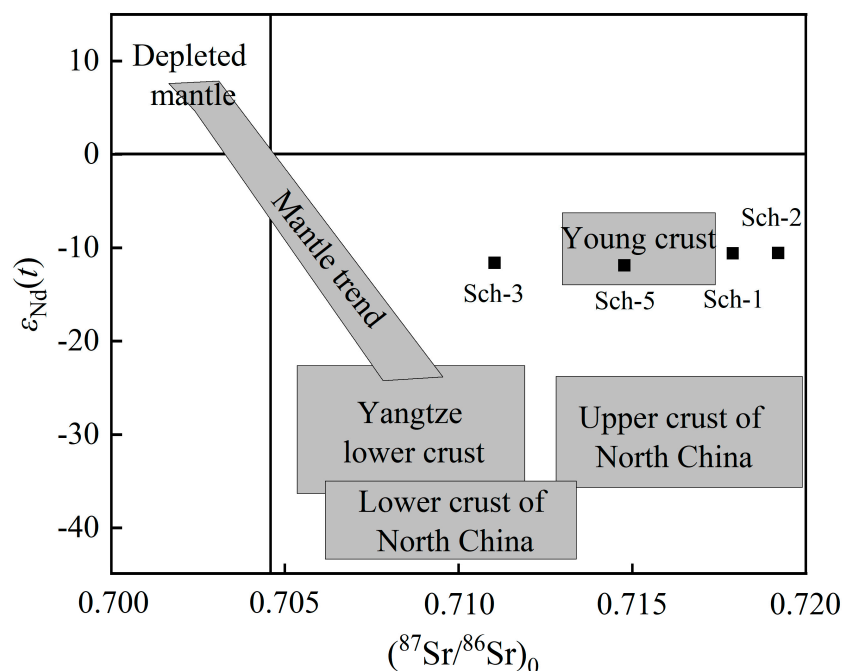


Figure 11. A diagram illustrating the $(^{87}\text{Sr}/^{86}\text{Sr})_0\text{-}\epsilon_{\text{Nd}}(t)$ relationship with scheelite from Xuebaoding, indicating the predominant occurrence in the upper crust and partial presence in the younger crust section according to predecessors [39].

6. Conclusions

- (1) Scheelite from Xuebaoding exhibits a weak dichroism in a light yellow tone, and the density decreases with increasing Mo content. In addition, L.W. displays inert fluorescence, while S.W. demonstrates moderate to strong blue white fluorescence. Clear color bands and ring structures are observed inside. The scheelite crystals possess crystallinity with a distinct granular structure, and the interference color falls into three categories: light blue, blue, and yellow. The mineral components are relatively concentrated, primarily composed of muscovite and illite as associated mineral along with minor amounts of fluorite and calcite.
- (2) The mass ratio of the main chemical components WO_3 and CaO in scheelite closely approximates or exceeds the ideal value. The content of trace elements Si, Sr, and Fe is relatively high. The REE composition indicates a higher enrichment of LREE compared to HREE, with significant Eu negative anomalies and insignificant Ce anomalies. The formation age of scheelite can be traced back to the Early Jurassic period, with an age of 183 Ma.
- (3) The scheelite from Xuebaoding was formed in a low sodium environment, and the rare earth patterns exhibit the tetrad effect, which is influenced by the distribution coefficient of rare earths in the hydrothermal solution rather than crystal chemistry. The genesis type corresponds to A type granite, which serves as the host rock for scheelite ore. Sr-Nd isotopes indicate that the material source primarily originates in the upper crust, with some coming from the young crust.

Author Contributions: Q.C. and M.S. designed the experiments; Q.C. and Y.Y. performed the experiments; S.M. resources; H.L. investigation; Q.C. analyzed the data and wrote the paper. All authors have read and agreed to the published version of the manuscript.

Funding: The research was funded by National Natural Science Foundation of China (Grant No. 42002156), Natural Science Foundation of Hebei Province of China (Grant No. D2021403015), Science and Technology Project of Hebei Education Department (Grant No. QN2021027), Hebei GEO University National Pre-research Project Funding (Grant No. KY2024YB01), Graduate Innovation Project of Hebei Province of China (Grant No. CXZZSS2023134), the Opening Foundation of Hebei Key Labo-

ratory of Strategic Critical Mineral Resources (Grant No. HGU-SCMR2310 and HGU-SCMR2309). The APC was funded by [National Natural Science Foundation of China], grant number [42002156], [Natural Science Foundation of Hebei Province of China], grant number [D2021403015], and [Science and Technology Project of Hebei Education Department], grant number [QN2021027].

Data Availability Statement: All data are contained within the work.

Acknowledgments: We are grateful to the Editor-in-Chief and the Academic Editors, as well as two anonymous reviewers for their constructive comments and suggestions that greatly improve this manuscript.

Conflicts of Interest: The authors declare no conflict of interest.

References

- Li, S.Y. *Crystallography and Mineralogy*; Geological Publishing House: Beijing, China, 2008; p. 284. (In Chinese)
- Palmer, M.C.; Scott, J.M.; Luo, Y.; Sakar, C.; Pearson, D.G. In-situ scheelite LASS-ICPMS reconnaissance Sm-Nd isotope characterisation and prospects for dating. *J. Geochem. Explor.* **2021**, *224*, 106760. [[CrossRef](#)]
- Poulin, R.S.; McDonald, A.M.; Kontak, D.J.; McClenaghan, M.B. On the relationship between cathodoluminescence and the chemical composition of scheelite from geologically diverse ore-deposit environments. *Can. Mineral.* **2016**, *54*, 1147–1173. [[CrossRef](#)]
- Poulin, R.S.; Kontak, D.J.; McDonald, A.; McClenaghan, M.B. Assessing scheelite as an ore-deposit discriminator using its trace-element and REE chemistry. *Can. Mineral.* **2018**, *56*, 265–302. [[CrossRef](#)]
- Scanlan, E.J.; Scott, J.M.; Wilson, V.J.; Stirling, C.H.; Reid, M.R.; Roux, P.J. In situ $^{87}\text{Sr}/^{86}\text{Sr}$ of scheelite and calcite reveals proximal and distal fluid-rock interaction during orogenic W-Au mineralization, Otago Schist, New Zealand. *Econ. Geol.* **2018**, *113*, 1571–1586. [[CrossRef](#)]
- Song, G.X.; Xiong, Y.X. Advances and Prospects of Scheelite Genetic Mineralogy. *Shandong Land Resour.* **2021**, *37*, 1–9.
- Liu, Y. Mineralogical characteristics and genetic mechanism of the Xuebaoding deposit in northwestern Sichuan Province. *Acta Petrol. Mineral.* **2017**, *36*, 549–563.
- Wu, D.W.; Li, B.H.; Du, X.F.; Dong, X.Y.; Fu, T.Y.; Xu, L. Fluid inclusion study and its geological significance on Xuebaoding W-Sn-Be deposit, Sichuan. *Miner. Depos.* **2015**, *34*, 745–756.
- An, N.; Guo, Q.F.; Liao, L.B. Gemological and Spectroscopic Characteristics of Scheelite from Xuebaoding, Sichuan. In Proceedings of the China International Jewelry and Jewelry Academic Exchange Conference, Beijing, China, 13 November 2019; pp. 173–176.
- Liu, Y.; Deng, J.; Xing, Y.Y.; Jiang, S.Q. Vibrational Spectra of Scheelite and Its Color Genesis. *Spectrosc. Spectr. Anal.* **2008**, *28*, 121–124.
- Li, J.K.; Liu, S.B.; Wang, D.H.; Fu, X.F. Metallogenic epoch of Xuebaoding W-Sn-Be deposit in northwest Sichuan and its tectonic tracing significance. *Miner. Depos.* **2007**, *26*, 557–562.
- Cao, Z.M.; Li, Y.G.; Ren, J.G.; Li, B.H.; Xu, S.J.; Wang, R.C.; Zheng, L.C.Y.; Jin, T.B.Z.; Xiao, L.X.Y. Characteristics and tracing and dating of volatile ore-forming fluids in the Xuebaoding beryl scheelite vein deposit. *Sci. China (Ser. D)* **2002**, *32*, 64–72.
- Li, B.H.; Cao, Z.M.; Li, Y.G.; Yi, H.S. CO₂ from Fluid Inclusions in Xuebaoding W-Sn-Be Deposit and Its Mineralization Significance. *Miner. Depos.* **2002**, *21*, 397–400.
- Zhu, X.X.; Liu, Y. Chemical Composition of Minerals in Xuebaoding W-Sn-Be Deposit, Sichuan Province: Constraints on One Genesis. *Rock Miner. Anal.* **2021**, *40*, 296–305.
- Zhang, B.L. *System Gemology*; Geological Publishing House: Beijing, China, 2006; pp. 523–524. (In Chinese)
- Li, M.R.; Wang, H.L.; Li, B.; Che, W.F.; Liang, D.Y.; Meng, Q.B. Mineralogical features, crystal structure, and floatability of the Mo-bearing scheelite. *Acta Metall. Sin.* **2022**, *42*, 213–221.
- Sun, S.S.; McDonough, W.F. Chemical and isotopic systematics of oceanic basalts: Implications for composition and processes. In *Magmatism in the Ocean Basin*; Geological Society Special Publication: London, UK, 1989; Volume 42, pp. 313–345.
- Brugger, J.; Bettioli, A.A.; Costa, S.; Lahaye, Y.; Bateman, R.; Lambert, D.D.; Jamieson, D.N. Mapping REE distribution in scheelite using luminescence. *Mineral. Mag.* **2000**, *64*, 891–903. [[CrossRef](#)]
- Nevin, C.G.; Pandalai, H.S. Rare earth element geochemistry and fluid characteristics of scheelite in the Hutti gold deposit, Hutti-Maski schist belt, Raichur district, Karnataka, India. *J. Asian Earth Sci.* **2020**, *189*, 104–161. [[CrossRef](#)]
- Bell, K.; Anglin, C.D.; Franklin, J.M. Sm-Nd and Rb-Sr isotope systematics of scheelites: Possible implications for the age and genesis of vein-hosted gold deposits. *Geology* **1989**, *17*, 500–504. [[CrossRef](#)]
- Eichhorn, R.; Höll, R.; Jagoutz, E.; Schärer, U. Dating scheelite stages: A strontium, neodymium, lead approach from the Felhertal tungsten deposit, Central Alps, Austria. *Geochim. Et Cosmochim. Acta* **1997**, *61*, 5005–5022. [[CrossRef](#)]
- Vermeesch, P. IsoplotR: A free and open toolbox for geochronology. *Geosci. Front.* **2018**, *9*, 1479–1493. [[CrossRef](#)]
- Steiger, R.H.; Jäger, E. Subcommittee on geochronology: Convention on the use of decay constants in geo- and cosmochronology. *Earth Planet. Sci. Lett.* **1977**, *36*, 359–362. [[CrossRef](#)]
- Cohen, K.M.; Finney, S.C.; Gibbard, P.L.; Fan, J.-X. The ICS International Chronostratigraphic Chart. *Epis. J. Int. Geosci.* **2023**, *36*, 199–204. [[CrossRef](#)]

25. Liu, Y.; Deng, J.; Li, C.F.; Shi, G.H.; Zheng, A.L. Rare earth geochemistry and Sm-Nd isotope dating of the Xuebaoding scheelite deposit in Sichuan. *Chin. Sci. Bull.* **2007**, *52*, 1923–1929.
26. Nie, L.Q.; Zhou, T.F.; Zhang, Q.M.; Zhang, M.; Wang, L.H. Trace elements and Sr-Nd isotopes of scheelites: Implications for the skarn tungsten mineralization of the Donggushan deposit, Anhui Province. *Acta Petrol. Sin.* **2017**, *33*, 3518–3530.
27. Ren, K.D.; Zhang, D.Y.; Meng, X.; Zhang, F.; Wang, J.; Xi, X.C.; Zhang, Y.W.; Su, H.B. Enrichment mechanism of rare earth (REE) of high-Mo scheelite in Guilinzheng deposit from Jiangnan tung mineralization belt and its geological significance. *Miner. Depos.* **2022**, *41*, 859–877.
28. Wei, Y. The Mineral Characteristics and Metallogenic Mechanism of Scheelite in the Zhaishang Gold Deposit in the Western Qinling Orogenic Belt. Master's Thesis, China University of Geosciences, Beijing, China, 2014.
29. Xue, Y.S.; Liu, X.W.; Hu, X.S.; Cun, X.N.; Yang, H.T. Scheelite geochemical signature and calcite Sm-Nd dating of the Xianggou Au-W deposit in south Qinling orogen, central China: Constraints, on the ore-forming process. *Geol. Chin.* **2021**, *48*, 1818–1837.
30. Peng, J.T.; Wang, C.; Li, Y.L.; Hu, A.X.; Lu, Y.L.; Chen, X.J. Geochemical characteristics and Sm-Nd Geochronology of scheelite in the Baojinshan ore district, central Human. *Acta Petrol. Sin.* **2021**, *37*, 665–682.
31. Masuda, A.; Kawakami, O.; Dohmoto, Y.; Takenaka, T. Lanthanide tetrad effects in nature: Two mutually opposite types, W and M. *Geochem. J.* **1987**, *21*, 119–124. [[CrossRef](#)]
32. Irber, W. The lanthanide tetrad effect and its correlation with K/Rb, Eu/Eu*, Sr/Eu, Y/Ho, and Zr/Hf of evolving peraluminous granite suites. *Geochim. Et Cosmochim. Acta* **1999**, *63*, 489–508. [[CrossRef](#)]
33. Monecke, T.; Kempe, U.; Monecke, J.; Sala, M.; Wolf, D. Tetrad effect in rare earth element distribution patterns: A method of quantification with application to rock and mineral samples from granite-related rare metal deposits. *Geochim. Et Cosmochim. Acta* **2002**, *66*, 1185–1196. [[CrossRef](#)]
34. Zhao, Z.H.; Bao, Z.W.; Qiao, Y.L. A peculiar composite M- and W-type REE tetrad effect: Evidence from the Shuiquangou alkaline syenite complex, Hebei Province, China. *Chin. Sci. Bull.* **2010**, *55*, 1474–1488. [[CrossRef](#)]
35. Zhou, J.Y.; Tan, H.Q.; Gong, D.X.; Zhu, Z.M.; Luo, L.P. Wulaxi Aluminous A-type Granite in Western Sichuan, China: Recording Early Yanshanian Lithospheric Thermo-upwelling Extension of Songpan-Garce Orogenic Belt. *Geol. Rev.* **2014**, *60*, 348–362.
36. Whalen, J.B.; Currie, K.L.; Chappell, B.W. A-type granites: Geochemical characteristics, discrimination and petrogenesis. *Contrib. Mineral. Petrol.* **1987**, *95*, 407–419. [[CrossRef](#)]
37. Song, G.X.; Qin, K.Z.; Li, G.M.; Evans, N.J.; Chen, L. Scheelite elemental and isotopic signatures: Implications for the genesis of skarn-type W-Mo deposits in the Chizhou Area, Anhui Province, Eastern China. *Am. Mineral.* **2014**, *99*, 303–317. [[CrossRef](#)]
38. Shao, J.A.; Mou, B.L.; Zhu, H.Z.; Zhang, L.Q. Material source and tectonic settings of the Mesozoic mineralization of the Da Higgan Mts. *Acta Petrol. Sin.* **2010**, *26*, 649–656.
39. Guo, Z.J.; Li, J.W.; Huang, G.J.; Guan, J.D.; Dong, X.Z.; Tian, J.; Yang, X.C.; She, H.Q.; Xiang, A.P.; Kang, Y.J. Sr-Nd-Pb-Hf isotope characteristics of ore-bearing granites in the Honghuaerji scheelite deposit, Inner Mongolia. *Geol. Chin.* **2014**, *41*, 1226–1241.

Disclaimer/Publisher's Note: The statements, opinions and data contained in all publications are solely those of the individual author(s) and contributor(s) and not of MDPI and/or the editor(s). MDPI and/or the editor(s) disclaim responsibility for any injury to people or property resulting from any ideas, methods, instructions or products referred to in the content.